Optical and Quantum Electronics **10** (1978) 17–29

The cladded parabolic-index profile waveguide: analysis and application to stripe-geometry lasers

M. J. ADAMS
Department of Electronics, The University, Southampton, SO9 5NH

Received 10 June 1977; revised 8 August 1977

A two-dimensional real waveguide having a parabolic distribution of dielectric permittivity in the core region, flanked by cladding layers of constant refractive index is proposed as a model for a class of stripe-geometry injection lasers. The model is analysed by a series-solution method and results are given in terms of plots of normalized propagation constant, near-field filling factor, and far-field half-angle, all versus normalized frequency. These results are compared with those for the alternative models of (a) a homogeneous core waveguide, and (b) a medium whose dielectric permittivity varies quadratically with position throughout the whole of space.

Apart from the series-solution method which was employed, a survey is included of other techniques available for analysing this waveguide model. These include perturbation theory, variational analysis, an exact solution of the scalar wave equation, and the WKB approximation.

1. Introduction

Progress in the development of the injection laser towards the goal of a useful, controllable, and long-lived source for optical fibre communications systems has depended heavily on improved understanding of its electromagnetic modal behaviour. The achievement of CW operation at room temperature [1, 2] and, more recently, single-mode output [3, 4] have come about as a result of a detailed knowledge of the waveguiding action occurring in these devices both perpendicular and parallel to the junction plane. In addition, recently developed structures [3–10] utilizing this knowledge promise linear output characteristics, low noise behaviour, and very high slope efficiencies.

Theoretical models of the waveguiding behaviour normal to the junction plane in the laser have included the familiar 'step-index' case (homogeneous active layer), [11, 12] the linearly-graded dielectric guide [13, 14], the extended parabolic index medium [15], and the Epstein layer theory [16–21]. Within the junction plane, the models used have largely centred on the step-index [22, 23] and parabolic profile [15, 24–26] guides, and the latter has yielded a powerful technique for the interpretation of experimental measurements in stripe-geometry devices. The combined problem of the guiding action perpendicular and parallel to the junction plane has been treated by a parabolic variation of dielectric permittivity in both directions [15, 24], by the Marcatili approximation [27] for the step-index case [23, 28], or more generally by the effective-index method [8, 29, 30]. In this latter theory the guiding action produced by the epitaxial layers is treated by a step-index model at each position along the active layer, and the resulting propagation constant is used to calculate an effective refractive index for use in the solution of the guiding problem associated with the stripe-geometry. The effective index thus retains the characteristic dielectric profile in the plane of the epitaxial layers due to the stripe-geometry, whilst also including the guiding effect transverse to the layers. This approach has the advantage that for most cases of interest the problem reduces to the two-dimensional waveguide due to the stripe-geometry or other guiding structure introduced in the junction plane.

In spite of the successful use of the parabolic-index profile as a model for the guide in the plane of the junction, there remain some problems associated with this technique. There are, for example, instances in the literature of experimental observations which may not be accounted for by the

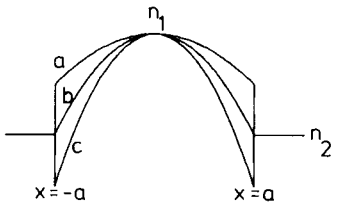

Figure 1 Refractive index profile for the cladded-parabolic waveguide.
(a) $\rho < 1$
(b) $\rho = 1$
(c) $\rho > 1$

Hermite–Gaussian modes characteristic of this model [31, 32]. From a theoretical standpoint there are at least two disturbing features of the model:

(i) the neglect of the full vector nature of the electromagnetic field distributions, and

(ii) the neglect of the surrounding homogeneous 'cladding' regions of the guide.

With reference to (i), the conventional theory neglects the term in the wave equation containing the gradient of the dielectric permittivity. A number of authors [33–38] have examined the effect of this omission, and it has been concluded on the basis of perturbation theory [35] that for most practical cases this constitutes a reasonable approximation, with the exception of the values for group velocity of the lowest-order TM modes. Since the group velocity is of little interest for studies of the injection laser, we may assume that point (i) is a reasonable justified approximation.

As regards point (ii) above, although a number of analyses of the 'cladded parabolic profile' have been published [39–49] there has been as yet no systematic study of the implications for the stripe-geometry laser. It is the purpose therefore of the present contribution to explore in some detail the effects of the cladding regions and to compare the cladded parabolic profile with both the infinitely-extensive parabolic medium and the step-index waveguide. The results will be presented in the form of normalized propagation constant and near- and far-field filling factors in order to facilitate comparison with experimental results.

2. The cladded parabolic profile waveguide

We consider here a real dielectric waveguide whose profile is shown schematically in Fig. 1, consisting of a central 'core' region where the dielectric permittivity has a quadratic dependence on position, lying between two 'cladding' regions of homogeneous dielectric. The extension to the corresponding waveguide of complex permittivity will be given in a future paper. The refractive index variation $n(x)$ with position x normal to the waveguide axis is given by

$$n^2(x) = \begin{cases} n_1^2\left[1 - 2\Delta\rho\left(\dfrac{x}{a}\right)^2\right], & |x| \leqslant a \qquad (1a) \\ n_1^2\left[1 - 2\Delta\right] \equiv n_2^2, & |x| > a \qquad (1b) \end{cases}$$

where n_1 = refractive index at core centre ($x = 0$), n_2 = cladding refractive index, a = guide half-width, $2\Delta = (n_1^2 - n_2^2)/n_1^2$, and ρ is a parameter introduced [39] to permit an index discontinuity at the core–cladding interface. The cases $\rho < 1$, $\rho = 1$ and $\rho > 1$ are indicated on the figure; the case $\rho = 0$ corresponds to the familiar step-index waveguide. This model is to be contrasted with the infinitely-extensive parabolic guide where Equation 1a (with $\rho = 1$) is allowed to hold for all values of x, so that all effects of the cladding layers are ignored.

Quite recently several theoretical treatments of the cladded parabolic waveguide, for both the slab and cylindrical geometry, have appeared [39–49]; the methods employed include perturbation theory [40–41], variational analysis [39, 42–46], an exact solution [47], and WKB methods [47–49]. These approaches are reviewed in Appendices 1–4, respectively. Since our interest here lies principally in a fast, efficient method of solution for the situation relatively close to cut-off of the lowest-order modes, for the reasons given in the Appendices we opt for a simplified series solution method based on the approach used for optical fibre analysis by Dil and Blok [50] and Gambling *et al.* [51]. For simplicity

TABLE I The three waveguide models and mathematical details of their solutions

	Step-index	Extended-parabola	Cladded-parabola
Dielectric profile	$n^2(x) = \begin{cases} n_1^2 (\lvert x\rvert \leqslant a) \\ n_2^2 (\lvert x\rvert > a) \end{cases}$	$n^2(x) = n_1^2\left[1 - 2\Delta\left(\frac{x}{a}\right)^2\right]$ (all x)	$n^2(x) = \begin{cases} n_1^2\left[1 - 2\Delta_2\left(\frac{x}{a}\right)^2\right] (\lvert x\rvert \leqslant a) \\ n_2^2 \qquad\qquad (\lvert x\rvert > a) \end{cases}$
Field distributions	$\cos\left(\frac{ux}{a}\right) (\lvert x\rvert \leqslant a)$	$H_p\left[\frac{(\sqrt{v}x)}{a}\right] \exp\left(-\frac{vx^2}{2a^2}\right)$	$\sum_{n=0}^{N} a_n \left(\frac{x}{a}\right)^n \quad (\lvert x\rvert \leqslant a)$
	$\cos u\, e^{w(1-x/a)} (\lvert x\rvert > a)$	$(p = 0, 1, 2, \ldots$ all $x)$;	$\left(\sum_{n=0}^{N} a_n\right) e^{w(1-x/a)} (\lvert x\rvert > a)$
			$a_n = \frac{\rho v^2 a_{n-4} - u^2 a_{n-2}}{n(n-1)}$
			Even order modes: $a_0 = 1, a_{2j+1} = 0$ (all j)
			Odd order modes: $a_1 = 1, a_{2j} = 0$ (all j)
Eigenvalue equation	$\tan(2u) = \frac{2uw}{u^2 - w^2}$	$u^2 = v(2p + 1)$	$\sum_{n=0}^{N} n a_n = -w \sum_{n=0}^{N} a_n$
Filling factor, Γ	$\frac{v + \sqrt{b}}{v + 1/\sqrt{b}}$	$\sqrt{\frac{v}{\pi}} \frac{\int_0^1 [H_p(\sqrt{v}y)]^2 e^{-vy^2} dy}{2^{p-1} p!}$	$\frac{1}{1 + \left[\left(\sum_{n=0}^{N} a_n\right)^2 \Big/ 2w \sum_{n=0}^{N}\sum_{m=0}^{N} \left(\frac{a_n a_m}{n + m + 1}\right)\right]}$
		$p = 0$: erf $\sqrt{v}$	
Equation for far-field filling factor γ (for zero-order mode) in terms of $y = ka \sin\theta_{1/2} = \gamma v$	$\left\lvert \frac{wu^2(w\cos y - y \sin y)}{(u^2 - y^2)(w^2 + y^2)} \right\rvert^2 = \frac{1}{2}$	$y^2 = 2v \ln\sqrt{2}$	$\left\lvert \sum_{n=0}^{N} a_n \left(\frac{1}{w} + \frac{1}{n+1}\right) \Big/ \frac{(w\cos y - y \sin y)}{(w^2 + u^2)} \sum_{n=0}^{N} a_n + \sum_{n=0}^{N} a_n I_n \right\rvert^2 = 2$
			$I_n = \int_0^1 z^n \cos(yz)\, dz$

we restrict attention here to the weakly-guiding situation ($\Delta \ll 1$) so that TE and TM modes are degenerate. Table I gives expressions for the field distributions and eigenvalue equation obtained by this method; the corresponding results for the step-index and extended-parabolic cases are also shown for the sake of completeness and convenience of reference. It was found for the cases considered here that the convergence of the series was such that an adequate degree of accuracy was achieved in about 20–30 terms. Solution of the appropriate eigenvalue equation shown in Table I was easily effected numerically.

The notation employed in Table I and throughout the paper uses the normalized variables originally proposed for optical fibres and now widely used for all dielectric waveguides [22, 30, 52, 53]:

$$u^2 = a^2(k^2n_1^2 - \beta^2) \tag{2}$$

$$v^2 = a^2k^2(n_1^2 - n_2^2) \tag{3}$$

$$w^2 = v^2 - u^2 \tag{4}$$

$$b = w^2/v^2 \tag{5}$$

where β is the longitudinal propagation constant, $k = 2\pi/\lambda$, and λ is the wavelength in air. The quantity b defined in Equation 5 represents a normalized propagation constant, since in the weakly-guiding situation considered here b is approximately proportional to β [52].

Results for the three waveguide models of Table I are given in Figs. 2, 3 and 5 and in Table II; for simplicity we restrict attention to the important case $\rho = 1$ in Equation 1a. Fig. 2 shows the variation of the normalized propagation constant b with normalized frequency v for the lowest-order mode in each guide. The normalization is such that each mode in a waveguide of a given profile is represented by a single line on the b–v plot. Cut-off for each mode occurs when $b = 0 = w$, and far from cut-off the value of b tends asymptotically to 1. The step-index results shown in Fig. 2 are well-known [53] as is the curve for the extended parabolic medium. However, it should be noted that the condition $w = 0$ for this latter case does not correspond physically to a cut-off condition, since the effects of the cladding regions are omitted from this model. In other words the field distributions at $w = 0$ do not display any characteristics corresponding to cut-off and this leads, as we shall see later, to considerable errors in the computation of filling factors and far-fields over a range of v-values for each mode. The cladded-parabolic model described above corrects these errors and gives realistic field distributions for all v's including the situation close to cut-off. In particular it is clear that the lowest-order mode has no cut-off, as anticipated from physical considerations. The cut-off values of v for the first six modes of the three models discussed are given in Table II. Also shown are the approximate analytic results for the mode cut-offs of the cladded-parabolic profile obtained from a recently-proposed variational formulation of the problem [39] (see Appendix 2).

It is relevant to enquire at this stage how these results would be changed in the case of an index discontinuity of the core–cladding interface. The calculations for this situation show: (i) for $\rho < 1$ in Equation 1a, the b–v curves shift towards the step-index case, since the profile now more closely

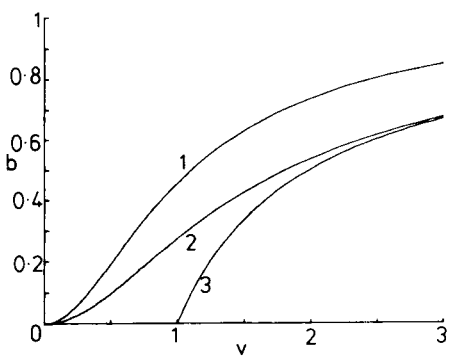

Figure 2 Normalized propagation constant b versus normalized frequency v for the lowest-order mode in the cases:

1 – step-index profile
2 – cladded parabolic-index profile
3 – extended parabolic-index profile

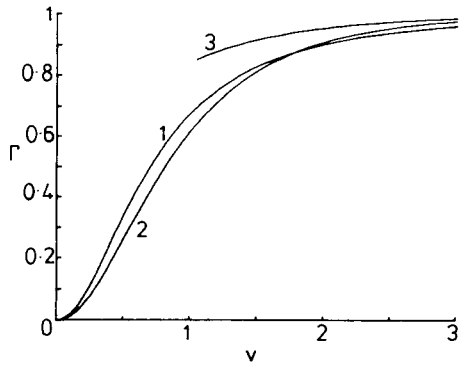

Figure 3 Filling factor, Γ, versus normalized frequency v for the lowest-order mode in the cases:

1 – step-index profile
2 – cladded parabolic-index profile
3 – extended parabolic-index profile

resembles the step-index one, and (ii) for $\rho > 1$ the curves shift in the opposite direction. For higher-order modes these changes are accompanied by corresponding shifts of the cut-offs, e.g. for $\rho = 0.5$ the cut-offs of Table II, column 4, for modes 1–3 are diminished by about 12–15%.

3. Near-field filling factor and threshold calculations

3.1. Filling factor

For interpretation of stripe-geometry laser observations and calculations of threshold currents, an essential pre-requisite is a knowledge of the near-field filling factor Γ [54–57] defined as

$$\Gamma = \frac{\text{Power in core}}{\text{Total power}} = \int_{-a}^{a} |E(x)|^2 dx \Big/ \int_{-\infty}^{\infty} |E(x)|^2 dx \tag{6}$$

where $E(x)$ is an electric field component at position x. Appropriate expressions for Γ for the three waveguide models discussed are given in Table I. Previous calculations of Γ have been made [54–57] only for specific device configurations concentrating on the waveguide perpendicular to the junction plane and without the generality of the normalized units used here. Hence Fig. 3 shows plots of Γ versus v for the lowest-order mode in each of the three guides discussed. From a value of zero at mode cut-off, the filling factors increase in a way characteristic of the waveguide dielectric profile and converge asymptotically for high v. As anticipated earlier, the infinite parabolic medium yields values markedly different from the cladded parabolic guide over a substantial range of v-values.

3.2. Optimal waveguide parameters for minimum threshold current

In order to give an idea of the use of Γ in practical calculations, we may apply these results to the determination of optimal laser structures for minimum threshold currents. The general threshold relation may

TABLE II Mode cut-off v-values for the first six modes of the waveguide models of Table I

Mode number	Step-index	Extended-parabolic profile	Cladded-parabolic profile	
			Series solution	Analytic variational result (Equation A.12)
0	0	1	0	0
1	1.571	3	2.263	2.221
2	3.142	5	4.287	4.443
3	4.712	7	6.298	6.664
4	6.283	9	8.304	8.886
5	7.854	11	10.308	11.107

be written in terms of Γ, the nett gain per unit length in the core region, g, the loss α in the cladding regions, and the end-loss $\ln(1/R)/L$ (R = facet reflectivity, L = cavity length) as:

$$g\Gamma = \alpha(1-\Gamma) + \frac{1}{L}\ln\left(\frac{1}{R}\right). \tag{7}$$

Hence the threshold current I_{th} may be found via the relation [56, 58, 59]

$$I_{th} = Ca(g - g_0) \tag{8}$$

where C is a constant and g_0 is a loss corresponding to cavity transparency. In the situation frequently encountered $g \gg g_0$, the calculation may proceed to simplified results for the two cases:

(i) dominant loss due to absorption in the cladding, or

(ii) dominant end-loss.

In case (i) we find that the minimum threshold current is achieved for the minimum value of the normalized quantity $v(1-\Gamma)/\Gamma$, whereas in case (ii) we require instead to minimize v/Γ. For the step-index waveguide these situations correspond respectively to those considered for guiding normal to the junction plane (i) of homostructures by Anderson [11], and (ii) of double heterostructures by Unger [60]. For case (i) we find that the threshold expression is a monotonic decreasing function of v so that we need only choose always the highest value of v subject to the non-existence of higher-order modes, namely $\pi/2$ for the step guide and 2.26 for the cladded parabolic profile. For case (ii) on the other hand, a minimum value of the threshold function exists in each case, leading to optimum v-values of 0.71 for the step guide and 0.91 for the cladded parabola.

4. Far-field half-angle for the zero-order mode

The other principle quantity required for laser analysis is the far-field pattern, especially that of the lowest-order mode. The appropriate expression for the far-field $I(\theta)$ at angle θ in terms of an electric field component $E(x)$ is [61–66]

$$\frac{I(\theta)}{I(0)} = g(\theta)\left|\frac{\int_{-\infty}^{\infty} E(x)\exp(ika\sin\theta)\,dx}{\int_{-\infty}^{\infty} E(x)\,dx}\right|^2 \tag{9}$$

where $g(\theta)$ is an obliquity factor, allowing for reflected radiation at the facet, whose form has been given elsewhere [61–66]. For θ less than about 20^0 the value of $g(\theta)$ remains close to unity; this restriction is usually satisfied for the beam divergence due to a stripe-geometry contact. For larger angles θ, an approximate formula has been given by Lewin [65] which converts the far-field half-angle calculated in the presence of the obliquity factor $g(\theta)$ to that deduced without $g(\theta)$. Hence, since the obliquity factor cannot be expressed in terms of the normalized variables used here and must be computed for each individual case, we restrict attention here to cases for which $g(\theta) = 1$, [8, 12, 55, 67, 68] and refer readers to Lewin's paper [65] for details of the conversion to the general half-angle expressions as noted above.

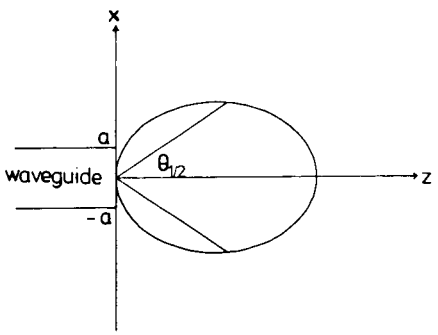

Figure 4 Schematic far-field of a slab waveguide, illustrating the definition of $\theta_{1/2}$ = half-angle to the half-power points.

In order to characterize the far-field we use half the angle to the half-power points in the far-field, as illustrated in Fig. 4, given by

$$\frac{I(\theta_{1/2})}{I(0)} = \frac{1}{2}. \tag{10}$$

Hence we may express the half-angle $\theta_{1/2}$ in terms of the naturally-occurring quantity $y = ak \sin \theta_{1/2}$, and the appropriate equations defining y for the zero-order mode are given in Table I. In order to produce a normalized plot whose values occur always between 0 and 1, in common with those of the variables b and Γ in Figs. 2 and 3, we define a new normalized parameter γ which may be thought of as a 'filling-factor' for the far-field:

$$\gamma = \frac{ak \sin \theta_{1/2}}{v} \equiv \frac{\sin \theta_{1/2}}{(n_1^2 - n_2^2)^{1/2}}. \tag{11}$$

Plots of γ versus v for the three waveguide models considered here are given in Fig. 5. Once again it is clear that use of the extended-parabolic profile leads to considerable deviations from the results of the cladded-parabolic profile. Use of the extended-parabolic profile for calculations of far-field half-angle (Fig. 5) and near-field filling factor (Fig. 3) clearly leads to strongly unphysical results. In addition it is clear both in Fig. 5 and Fig. 3 that the detailed differences between curves calculated for the step-index and cladded-parabolic profiles are sufficient to enable these curves to be used in interpreting experimental measurements in terms of the underlying waveguide structure.

5. Conclusions

The cladded parabolic-index profile waveguide has been proposed as a model for the electromagnetic confinement in the junction plane in stripe-geometry lasers. Results have been obtained for a real dielectric waveguide of this type in the form of normalized plots for the lowest-order mode. The plots show a normalized propagation constant, near-field filling factor, and a far-field filling factor (related to the far-field half-angle) all versus normalized frequency v. These results show the strong effect of the cladding layers for a range of v-values near mode cut-off. When compared to the results for the step-index guide and the extended parabolic-index medium the new model shows considerable departures. It is concluded that:

(i) the extended parabolic-index medium, although yielding simple analytical formulae which are very useful in interpretation of laser experiments, must be used with considerable caution over quite large ranges of normalized frequency v where it yields unphysical results.

(ii) the differences of structure in the curves for different waveguide models may be used as a diagnostic tool for determining the type of waveguide present.

The results presented are those for no index discontinuity at the core–cladding interface. In the case of a positive discontinuity (on the core-side of the interface) the normalized plots shift towards those for

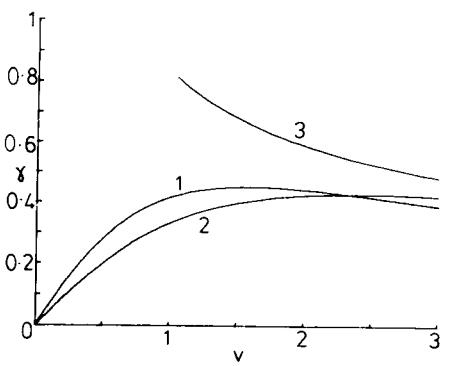

Figure 5 Far-field filling factor, γ, as defined in Equation 11, versus normalized frequency v for the lowest-order mode in the cases

1 – step-index profile
2 – cladded parabolic-index profile
3 – extended parabolic-index profile

the step-index guide; for a negative discontinuity the opposite behaviour occurs. Corresponding changes of the cut-offs for higher-order modes are also found.

As regards the analysis of the cladded parabolic guide, the simplest and most convenient method for low-order modes was found to be a series solution. The perturbation theory approach (Appendix 1) was found to hold over only limited ranges of v-values, although for $0 \leqslant v < 2$ it yielded useful results. The numerical variational analysis (Appendix 2.1.) yielded accurate results at all v-values but required fairly lengthy numerical computation involving the solution of 10 x 10 determinants. The analytical variational expression (Appendix 2.2) gave substantial errors for v greater than about 1.8, and its predictions for mode cut-offs became progressively worse with increasing mode number. Whilst the exact solution (Appendix 3) would give accurate results in principle, the practical difficulties of computing the necessary functions rendered an approximation necessary which resulted in some errors in the range $0 \leqslant v < 1$. For the WKB approximation (Appendix 4) it was found that the errors for the zero-order mode below $v = 2$ were such as to exclude this method from further consideration.

Finally, it should be emphasized that the results presented herein are for real dielectric waveguides and hence apply to injection lasers only in situations where the real waveguiding effect dominates over gain-guiding. Examples of such situations include the recent structures intended to yield linear output characteristics, including the channelled substrate buried heterostructure [8], the deep-diffused stripe laser [10], and the double stripe laser [72].

Appendix 1. Perturbation theory

It has been proposed [40, 41] that perturbation theory may provide useful results for the cladded parabolic profile waveguide in the two limiting situations (a) near cut-off, and (b) well above cut-off. In case (a) the unperturbed system is the step-index dielectric waveguide and the perturbation is produced by the grading of the dielectric profile, whilst in case (b) the unperturbed system is the infinite parabolic medium and the perturbation is a result of the cladding layers. It is the object of this Appendix to evaluate the accuracy and range of applicability of these two approximations.

To express the results for zero-order modes in terms of our normalized variables, we write the perturbed value of u (Equation 2) as

$$u^2 = u(0)^2 - u(1)^2 \tag{A.1}$$

where $u(0)$ is the value for the unperturbed system, and $u(1)$ is the correction resulting from first-order perturbation theory. For case (a) near cut-off, the result ([40], Equation 9) may be written as

$$u(1)^2 = -\frac{v^2}{(1+1/w)}\left[\frac{1}{3} + \frac{\cos 2u}{2u^2} + \frac{\sin 2u}{2u}\left(1 - \frac{1}{2u^2}\right)\right] \tag{A.2}$$

For case (b) far above cut-off the result ([40], Equation 5) becomes

$$u(1)^2 = v^2\left[\operatorname{erfc}(\sqrt{v})\left(\frac{1}{2v} - 1\right) + \frac{e^{-v}}{\sqrt{\pi v}}\right]. \tag{A.3}$$

The values of the normalized propagation constant b obtained by applying Equations A.1–A.3 together with the appropriate expressions for $u(0)$ for the step-index and extended-parabolic waveguides (see Table I) are shown plotted against v as solid lines on Fig. 6. Also shown (dotted line) is the series solution result for the cladded parabolic guide, taken from Fig. 2. It is clear that the ranges where the perturbation theory holds are rather restricted. For Equation A.2 the range $0 \leqslant v < 2$ gives perhaps reasonable accuracy in the determination of b, whilst Equation A.3 gives only a limited improvement over the results of the unperturbed extended-parabolic model and is only applicable with any degree of accuracy for v-values greater than about 2.

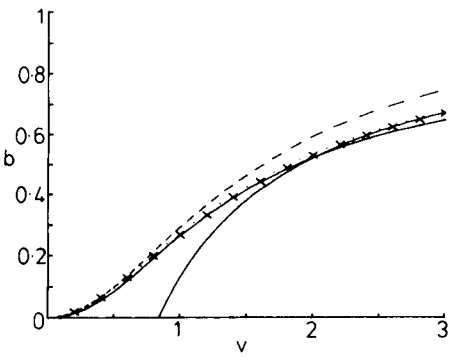

Figure 6 Normalized propagation constant b versus normalized frequency v for the lowest-order mode of the cladded parabolic profile waveguide calculated by the methods as follows:

solid line, perturbation theory (Equations A.2 and A.3)
dashed line, analytic variational analysis (Equation A.9)
crosses, numerical variational analysis (Equation A.6)
dotted line, series solution (final column of Table I)

Appendix 2. Variational analysis

A2.1. Numerical results

A recent variational formulation [39, 45] of the cladded waveguide problem is particularly suitable for use here. The technique was originally applied to analysis of optical fibre propagation but we modify it here to treat two-dimensional symmetric guides. For this case the function to be minimized $J(\psi)$ becomes [69]

$$J(\psi) = -\frac{w}{a}[\psi^2(a) + \psi^2(-a)] - \int_{-a}^{a}\left(\frac{\partial\psi(x)}{\partial x}\right)^2 dx + \int_{-a}^{a}[k^2n^2(x) - \beta^2]\,\psi^2(x)\,dx \qquad (A.4)$$

Restricting attention to even-order modes the problem may be solved by a Rayleigh–Ritz technique using as trial function [69]

$$\psi(x) = \sum_{\nu=0}^{N} a_\nu \frac{1}{\sqrt{a}}\cos\left(\frac{\nu\pi x}{a}\right). \qquad (A.5)$$

For the cladded parabolic profile of Equation 1 it is then possible to evaluate each of the terms on the right-hand side of Equation A.4. Applying the condition for minimization of the functional ($\partial J(\psi)/\partial a_\nu = 0$) yields the required eigenvalue equation in the form [45]

$$\det(S_{\mu\nu}) = 0 \qquad (A.6)$$

where [69]

$$S_\mu = \begin{cases} -w[1 + (-1)^{\mu+\nu}] + \left(u^2 - \dfrac{\mu^2\pi^2}{4}\right)\delta_{\mu\nu} - \rho C_{\mu\nu} & (\mu, \nu \text{ not both } 0) \\ -2w + 2u^2 - \rho C_{00} & (\mu = \nu = 0) \end{cases} \qquad (A.7)$$

with

$$C_{\mu\nu} = \begin{cases} \dfrac{v^2 4}{\pi^2}[1 + (-1)^{\mu+\nu}]\left[\dfrac{1}{(\mu-\nu)^2} + \dfrac{1}{(\mu+\nu)^2}\right] & \text{for } \mu \neq \nu \\ v^2\left(\dfrac{2}{\pi^2\mu^2} + \dfrac{1}{3}\right) & \text{for } \mu = \nu \neq 0 \\ v^2\frac{2}{3} & \text{for } \mu = \nu = 0. \end{cases}$$

Equation A.6 has been solved numerically [69] for a 10 x 10 determinant with $\rho = 1$ to give the b–v plot shown as crosses on Fig. 6. These results are in excellent agreement with those from the series solution described in the main text. However, for the low v-values considered there was a considerable saving in computer time in using the series rather than the variational technique and this was the principle factor in the choice of solution method.

A2.2. Analytic approximation

Thus far in this Appendix we have followed the variational analysis suggested for optical fibres by Okamoto and Okoshi [45]. However, these authors have also suggested an extension of this technique which results in a simplified closed-form expression for the eigenvalue equation [39]. This extension relies on the use of the re-formulated scalar wave equation in order to express the final term on the right-hand side of Equation A.4 in terms of integrals free from the refractive index profile $n(x)$. The method is applicable only to 'α-profiles' (i.e. of the form $n^2(x) = n^2[1 - 2\Delta\rho(x/a)^\alpha]$) and when adapted to even-order modes for the cladded parabolic guide in two dimensions yields the following re-formulation of the function, Equation A.4 [69]:

$$J(\psi) = -\frac{4}{3}\int_{-a}^{a}\left(\frac{\partial\psi}{\partial x}\right)^2 dx + \frac{2}{3}u^2\int_{-a}^{a}\psi^2(x)\frac{dx}{a^2} + \frac{2\psi^2(a)}{3a}[-3w + v^2(1-\rho)]. \tag{A.8}$$

Applying again the Rayleigh-Ritz solution with trial function as discussed above, the eigenvalue equation for even-order modes becomes [69]

$$\frac{u}{\sqrt{2}}\tan(u/\sqrt{2}) = \frac{3}{4}w. \tag{A.9}$$

Similarly, for odd-order modes an analogous derivation using as trial function

$$\psi(x) = \sum_{\nu=1}^{N} a_\nu \frac{1}{\sqrt{a}}\sin\left[\frac{\pi x}{a}(\nu - \tfrac{1}{2})\right] \tag{A.10}$$

the eigenvalue equation becomes [69]

$$\frac{u}{\sqrt{2}}\cot(u/\sqrt{2}) = -\frac{3}{4}w. \tag{A.11}$$

These results (Equations A.9 and A.11) form a clear analogy to the even and odd-order eigenvalue equations for the step-index guide (cf. Table I). They are easily solved numerically [69] and the result for the lowest-order mode has been plotted as a b–v curve on Fig. 6 (broken line). We see that whilst the agreement with the exact solution is good for v less than about 1.8, for values above this the curve gives very poor agreement and greatly overestimates the b-values. Presumably this is a result of the re-formulated variational expression (Equation A.8), although it is not as yet clear as to the exact cause of the discrepancy. Equations A.9 and A.11 yield also a simple expression for the cut-off values v_p of the modes in this approximation:

$$v_p = \frac{\pi}{\sqrt{2}}p \quad (p = 0, 1, 2, \ldots) \tag{A.12}$$

and these values are shown for the first six modes in the final column of Table II. It is clear that for increasing mode number the level of agreement with the 'exact' results (i.e. those from the series solution) becomes progressively worse. A further cause for concern with this variational analysis has been pointed out in [51] and is supported by the two-dimensional analogue presented here. It is that the electromagnetic field distributions resulting from this approximation reduce to those of the corresponding step-index guide whose v-value has been reduced by a factor $1/\sqrt{2}$. We conclude that the results of this approximate variational analysis must be used with considerable caution.

Appendix 3. Exact solution

The general solution of Hermite's differential equation has been applied to the cladded parabolic profile waveguide by Hashimoto [47]. This approach leads to solutions for the field components which are represented by contour integrals and hence not easily adaptable to computation of numerical results. However, an approximation is possible [47] which yields reasonably accurate results. Expressed in conventional normalised variables the eigenvalue equation for the p mode becomes

$$b = 1 - \frac{(2p + 1 + 2\Delta\nu_p)}{v} \tag{A.13}$$

where $\Delta\nu_p$ is given by the solution of [47]

$$\tan\left(\frac{\pi\Delta\nu_p}{2}\right) = \sqrt{\left(\frac{\pi}{2}\right)\frac{\sqrt{2}H_p'(\sqrt{2}v) + [(v - 2p - 1 - 2\Delta\nu_p)^{1/2} - v^{1/2}]\,H_p(\sqrt{2}v)}{\sqrt{2}h_p(\sqrt{2}v) + [(v - 2p - 1 - 2\Delta\nu_p)^{1/2} - v^{1/2}]\,h_p(\sqrt{2}v)}} \tag{A.14}$$

where the functions H_p, h_p represent respectively Hermite polynomials and Hermite functions of the second kind, and the primes represent differentiation with respect to the argument. A somewhat similar expression to Equation A.14 for $\Delta\nu_p$ has been derived by Hashimoto [48] via an argument based on the WKB approximation.

Numerical results of b versus v calculated from Equations A.13 and A.14 for the lowest-order mode ($p = 0$) are shown in Fig. 7 as crosses. For comparison, the series solution is again represented by a dotted line. The level of agreement is very good over most of the range except close to cut-off. In this region the errors are due to the use of the Hermite functions and polynomials in Equation A.14 rather than the integral representations of the exact solutions of Hermite's equation. In view of the nature of this difficulty we conclude that this approach is more suitable for use away from the regions close to mode cut-offs.

Appendix 4. WKB approximation

In its familiar application to optical waveguides, the WKB resonance condition (analogous to the Bohr–Sommerfeld quantization rule) when applied to the parabolic-index profile yields [70] the same results for the eigenvalue equation as that for the Hermite–Gaussian modes (see Table I). However, a recent analysis of the cladded parabolic-index profile optical fibre [49] uses a more extended version of the WKB approximation. This approach, which has already been applied to a study of leaky modes in graded-index fibres [71], utilizes the WKB fields in the core and cladding regions. An eigenvalue equation is derived in the usual way by matching the fields and their derivatives at the core-cladding interface. Applying this technique to the two-dimensional waveguide considered here, the eigenvalue equation becomes

$$\cot\left(\frac{u^2\pi}{2v}\right) = \left(\frac{v^2}{8w^3 - 2v^2}\right)\exp\left[\frac{u^2}{v}\ln\left(\frac{v + w}{u}\right) - w\right]. \tag{A.15}$$

The numerical solutions of this equation for the lowest-order mode are represented as squares on the b–v plot of Fig. 7. It is clear that the behaviour departs from the known solutions for v less than about 2 and gives meaningless results in the vicinity of the true cut-off. The method yields cut-off values for the p mode of

$$v_p = 2p - \frac{2}{\pi}\tan^{-1}(2) \equiv 2p - 0.705. \tag{A.16}$$

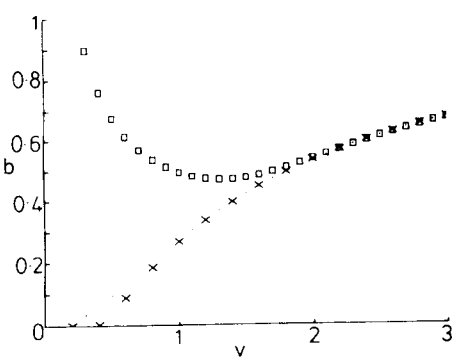

Figure 7 Normalized propagation constant b versus normalized frequency v for the lowest-order mode of the cladded parabolic profile waveguide calculated by the methods as follows:

crosses, approximation to the exact solution (Equations A.13 and A.14)
squares, WKB approximation (Equation A.15)
dotted line, series solution (final column of Table I)

Comparison with Table II shows that the results of Equation A.16 are considerably different from the accurate cut-off values. Although we therefore dismiss the WKB approximation as not suitable for further application to the problems considered here, it remains a valid and accurate tool for the analysis of multimode waveguides and especially for the computation of group velocities of higher-order modes [49].

Acknowledgements

I am indebted to J. J. Cynk for his work on the variational analysis summarized in Appendix 2, to R. Olshansky for a preprint of his paper [47], to D. N. Payne for his comments on the manuscript, and to the Science Research Council for the award of a research fellowship.

References

1. I. HAYASHI, M. B. PANISH, P. W. FOY and S. SUMSKI, *Appl. Phys. Lett.* **17** (1970) 109–11.
2. Zh. I. ALFEROV, V. M. ANDREEV, D. Z. GARBUZOV, Yu. V. ZHILYAEV, E. P. MOROZOV, E. L. PORTNOI and V. G. TRIOFIM, *Fiz. Tekh. Paluprov.* **4** (1970) 1826–9; also *Sov. Phys. Semicond.* **4** (1971) 1573–5.
3. H. NAMIZAKI, H. KAN, M. ISHII and A. ITO, *J. Appl. Phys.* **45** (1974) 2785–6.
4. M. YAMADA, H. NISHIZAWA and Y. SUEMATSU, *Trans. IECE Japan* **E59** (1976) 9–10.
5. T. TSUKADA, *J. Appl. Phys.* **45** (1974) 4899–906.
6. T. P. LEE, C. A. BURRUS, B. I. MILLER and R. A. LOGAN, *IEEE J. Quant. Elect.* **QE-11** (1975) 432–5.
7. R. D. BURNHAM, D. R. SCIFRES, J. C. TRAMONTANA and A. S. ALIMONDA, *ibid* **QE-11** (1975) 418–20.
8. P. A. KIRKBY and G. H. B. THOMPSON, *J. Appl. Phys.* **47** (1976) 4578–89.
9. H. KAWAGUCHI and T. KAWAKAMI, paper L-II-7 presented at IEEE International Semiconductor Laser Conference, Nemu-no-Sato, Japan 1976.
10. H. YONEZU, Y. MATSUMOTO, T. SHINOHARA, I. SAKUMA, T. SUZUKI, K. KOBAYASHI, R. LANG, Y. NANNICHI and I. HAYASHI, *Japan J. Appl. Phys.* **16** (1977) 209–10.
11. W. W. ANDERSON, *IEEE J. Quant. Elect.* **QE-1** (1965) 228–36.
12. M. J. ADAMS and M. CROSS, *Solid State Elect.* **14** (1971) 865–83.
13. J. HATZ and E. MOHN, *IEEE J. Quant. Elect.* **QE-3** (1967) 656–62.
14. K. A. SHORE and M. J. ADAMS, *Opt. Quant. Elect.* **8** (1976) 373–81.
15. T.H. ZACHOS and J. E. RIPPER, *IEEE J. Quant. Elect.* **QE-5**, (1969) 29–37.
16. K. UNGER, *Ann. Phys.* **19** (1969) 64–75.
17. R. G. ALLAKHVERDYAN, A. N. ORAEVSKII and A. F. SUCHKOV, *Fiz. Tekh. Poluprov.* **4** (1970) 341–46.
18. *Idem, Sov. Phys. Semicond.* **4** (1970) 277–81.
19. S. N. STOLYAROV, *Kvan. Elektron.* **2** (1972) 69–76.
20. *Idem, Sov. J. Quant. Elect.* **2** (1972) 144–9.
21. M. OSINSKI, *Arch. & Elekt. Ubertr.* **30** (1976) 223–4.
22. W. O. SCHLOSSER, *Bell Syst. Tech. J.* **52** (1973) 887–905.
23. M. CROSS and M. J. ADAMS, *Solid State Elect.* **15** (1972) 919–21.
24. F. R. NASH, *J. Appl. Phys.* **44** (1973) 4696–707.
25. D. D. COOK and F. R. NASH, *J. Appl. Phys.* **46** (1975) 1660–72.
26. B. W. HAKKI, *ibid.* **46** (1975) 2723–30.
27. E. A. J. MARCATILI, *Bell Syst. Tech. J.* **48** (1969) 2071–102.
28. E. VOGES, *Arch. & Elekt. Ubertr.* **28** (1974) 183–5.
29. R. M. KNOX and P. P. TOULIOS, Proc. of the Symposium on Submillimeter Waves (Ed. J. Fox) (Polytechnic Press, New York 1970) pp. 497–516.
30. G. B. HOCKER and W. K. BURNS, *Appl. Opt.* **16** (1977) 113–8.
31. H. S. SOMMERS, *J. Appl. Phys.* **46** (1975) 1844–6.
32. H. S. SOMMERS and J. K. BUTLER, *J. Appl. Phys.* **46** (1975) 2319–22.
33. Y. SUEMATSU and K. FURUYA, *Elect. Commun. Jap.* **54-B** (1971) 39–46.
34. M. MATSUHARA, *J. Opt. Soc. Amer.* **63** (1973) 135–8.
35. D. MARCUSE, *IEEE J. Quant. Elect.* **QE-9** (1973) 958–60.
36. R. YAMADE and Y. INABE, *J. Opt. Soc. Amer.* **64** (1974) 964–8.
37. A. K. GHATAK and L. A. KRAUS, *IEEE J. Quant. Elect.* **QE-10** (1974) 465–7.
38. K. THYAGARAJAN and A. K. GHATAK, *Opt. Commun.* **11** (1974) 417–21.
39. K. OKAMOTO and T. OKOSHI, *IEEE Trans.* **MTT-24** (1976) 416–21.
40. A. KUMAR, K. THYAGARAJAN and A. K. GHATAK, *IEEE J. Quant. Elect.* **QE-10** (1974) 902–4.
41. S. J. CHUA and B. THOMAS, *Opt. Quant. Elect.* **9** (1977) 15–32.

42. M. MATSUHARA, *J. Opt. Soc. Amer.* **63** (1973) 1514–17.
43. R. PREGLA, Proc. European Microwave Conference, Vol. I (Brussels, 1973), (University of Ghent, Belgium), paper B.5.2.
44. M. GESHIRO, M. OOTAKA, M. MATSUHARA and N. KUMAGAI, *IEEE J. Quant. Elect.* **QE-10** (1974) 647–9.
45. T. OKOSHI and K. OKAMOTO, *IEEE Trans.* **MTT-22** (1974) 938–45.
46. H.F. TAYLOR, *IEEE J. Quant. Elect.* **QE-12** (1976) 748–52.
47. M. HASHIMOTO, *Int. J. Electron.* **39** (1975) 579–82.
48. M. HASHIMOTO, *IEEE Trans.* **MTT-24** (1976) 404–9.
49. R. OLSHANSKY, *Appl. Optics* **16** (1977) 2171–74.
50. J. G. DIL and H. BLOK, *Opto-Electronics* **5** (1973) 415–28.
51. W. A. GAMBLING, D. N. PAYNE and H. MATSUMURA, *Elect. Lett.* **13** (1977) 139–40.
52. D. GLOGE, *Appl. Opt.* **10** (1971) 2252–8.
53. H. KOGELNIK and V. RAMASWAMY, *ibid.* **13** (1974) 1857–62.
54. I. HAYASHI, M. B. PANISH and F. K. REINHART, *J. Appl. Phys.* **42** (1971) 1929–41.
55. H. C. CASEY, M. B. PANISH and J. L. MERZ, *ibid.* **44** (1973) 5470–5.
56. B. W. HAKKI and T. L. PAOLI, *ibid.* **46** (1975) 1299– 306.
57. J. K. BUTLER and C.-S. WANG, *IEEE J. Quant. Elect.* **QE-12** (1976) 165–8.
58. M.J. ADAMS, *Solid State Elect.* **12** (1969) 661–9.
59. B. W. HAKKI, *J. Appl. Phys.* **44** (1973) 5021–8.
60. H. G. UNGER, *Arch. & Elekt. Ubertr.* **25** (1971) 539–40.
61. G. A. HOCKHAM, *Elect. Lett.* **9** (1973) 389–91.
62. L. LEWIN, *ibid.* **10** (1974) 134–5.
63. J. K. BUTLER and J. ZOROOFCHI, *IEEE J. Quant. Elect.* **QE-10** (1974) 809–15.
64. R. J. DE WAARD, *Elect. Lett.* **11** (1975) 11–12.
65. L. LEWIN, *J. Appl. Phys.* **46** (1975) 2323–4.
66. *Idem, IEEE Trans.* **MTT-23** (1975) 576–85.
67. H. KRESSEL, J. K. BUTLER, F. Z. HAWRYLO, H. F. LOCKWOOD and M. ETTENBERG, *R.C.A. Rev.* **32** (1971) 393–401.
68. P.A. KIRKBY and G. H. B. THOMPSON, *Opto-Electronics* **4** (1972) 323–34.
69. J. J. CYNK, Project Report, University of Southampton (1977).
70. A. H. HARTOG and M. J. ADAMS, *Opt. Quant. Elect.* **9** (1977) 223–32.
71. R. OLSHANSKY, *Appl. Opt.* **15** (1976) 2773–7.
72. P.A. KIRKBY, A. R. GOODWIN and R. S. BAULCOMB, presented at the conference 'Semiconductor Injection Lasers and their Applications', Cardiff, Wales (1977).